Monthly Notices
of the
ROYAL ASTRONOMICAL SOCIETY

MNRAS **453,** 4159–4174 (2015) doi:10.1093/mnras/stv1908

Gemini optical observations of binary millisecond pulsars

V. Testa,[1⋆] R. P. Mignani,[2,3⋆] C. Pallanca,[4] A. Corongiu[5] and F. R. Ferraro[4]

[1]*INAF – Osservatorio Astronomico di Roma, via Frascati 33, I-00040 Monteporzio, Italy*
[2]*INAF – Istituto di Astrofisica Spaziale e Fisica Cosmica Milano, via E. Bassini 15, I-20133 Milano, Italy*
[3]*Kepler Institute of Astronomy, University of Zielona Góra, Lubuska 2, PL-65-265 Zielona Góra, Poland*
[4]*Dipartimento di Fisica e Astronomia, Università degli Studi di Bologna, Viale Berti Pichat 6-2, I-40127 Bologna, Italy*
[5]*INAF – Osservatorio Astronomico di Cagliari, Via della Scienza 5, I-09047 Selargius, Italy*

Accepted 2015 August 17. Received 2015 August 16; in original form 2015 April 30

ABSTRACT

Millisecond pulsars (MSPs) are rapidly spinning neutron stars, with spin periods $P_s \lesssim 10$ ms, which have been most likely spun up after a phase of matter accretion from a companion star. In this work, we present the results of the search for the companion stars of four binary MSPs, carried out with archival data from the Gemini South telescope. Based upon a very good positional coincidence with the pulsar radio coordinates, we likely identified the companion stars to three MSPs, namely PSR J0614−3329 ($g = 21.95 \pm 0.05$), J1231−1411 ($g = 25.40 \pm 0.23$), and J2017+0603 ($g = 24.72 \pm 0.28$). For the last pulsar (PSR J0613−0200) the identification was hampered by the presence of a bright star ($g = 16 \pm 0.03$) at ∼2 arcsec from the pulsar radio coordinates and we could only set 3σ upper limits of $g = 25.0$, $r = 24.3$, and $i = 24.2$ on the magnitudes of its companion star. The candidate companion stars to PSR J0614−3329, J1231−1411, and J2017+0603 can be tentatively identified as He white dwarfs (WDs) on the basis of their optical colours and brightness and the comparison with stellar model tracks. From the comparison of our multiband photometry with stellar model tracks we also obtained possible ranges on the mass, temperature, and gravity of the candidate WD companions to these three MSPs. Optical spectroscopy observations are needed to confirm their possible classification as He WDs and accurately measure their stellar parameters.

Key words: stars: neutron – pulsars: general.

1 INTRODUCTION

Radio pulsars are interpreted as rapidly spinning and strongly magnetized neutron stars powered by their rotational energy. The most recent compilation (1.52) of the Australia National Telescope Facility (ATNF) Pulsar Catalogue[1] (Manchester et al. 2005) lists over 2300 radio pulsars. An important subgroup (∼270 objects) is that of the so-called millisecond pulsars (MSPs), characterized by very short spin periods ($P_s \lesssim 10$ ms), high spin stability ($\dot{P}_s \approx 10^{-18}$–$10^{-21}$ s s^{-1}), spin-down ages $P_s/2\dot{P}_s \sim 1$–10 Gyr, surface magnetic fields $B \sim 10^8$–10^9 G, and spin-down energy $\dot{E} \sim 10^{32}$–10^{36} erg s^{-1}.

A large fraction of MSPs (164) are in binary systems and are mostly located in the Galactic plane. The fact that many MSPs are found in binary systems supports the commonly accepted scenario for the formation and evolution of MSPs (the '*canonical recycling scenario*'; Alpar et al. 1982; Bhattacharya & van den Heuvel 1991). This suggests that MSPs form in binary systems from old (slowly rotating) pulsars and that, at a later stage, they are reaccelerated to millisecond spin periods as the result of mass accretion from their non-degenerate companion stars. The pathways to the MSPs are different according to the initial mass ratio and orbital separation of the components, which drives the length of the accretion processes (see e.g. Tauris 2011, 2015; Tauris, Langer & Kramer 2012).

The most common pathway leads to a companion star that has almost or completely lost its external layers (white dwarf; WD) orbiting a rapidly spinning pulsar (Alpar et al. 1982; Lyne et al. 1987; Bhattacharya & van den Heuvel 1991; Lorimer & Kramer 2005). In this case, the companion star is expected to be either an He WD of mass $0.1\,M_\odot \lesssim M_C \lesssim 0.5\,M_\odot$ or a more massive carbon–oxygen (CO) WD, of mass $0.5\,M_\odot \lesssim M_C \lesssim 1\,M_\odot$. When the companion star has not reached the WD stage yet it may be ablated by irradiation from the pulsar relativistic wind, which possibly leads to the formation of a solitary MSP. Two distinct families of binary MSPs with non-degenerate companions emerge according to the degree of the ablation processes (e.g. Roberts 2013). The first one is that of the so-called black widow (BW) MSPs, where the companion is a very low-mass star of $M_C \lesssim 0.1\,M_\odot$, almost fully ablated by the pulsar wind. The second one is that of the redbacks (RB) MSPs, where the companion is only partially ablated and has an higher mass of $M_C \sim 0.1$–$0.4\,M_\odot$. Therefore, the study of MSPs in binary systems is fundamental to understand the final stages of the binary

⋆E-mail: vincenzo.testa@oa-roma.inaf.it (VT); mignani@iasf-milano.inaf.it (RPM)

[1] http://www.atnf.csiro.au/research/pulsar/psrcat

Table 1. Coordinates, spin period P_s, and period derivative $\dot{P}_s$ of the observed MSPs, together with the inferred values of the spin-down age (τ), dipolar magnetic field (B), and rotational energy loss ($\dot{E}$), as derived from the ATNF pulsar data base. For the MSP coordinates, the number in parentheses represent the 1σ uncertainty on the last quoted digit. For those pulsars for which a proper motion has been measured (PSR J0613−0200 and J1231−1411), the values of $\dot{P}_s$, τ, B, and $\dot{E}$, have been corrected for the Shlowskhi effect.

Pulsar	α_{J2000} (hms)	δ_{J2000} (° ′ ″)	P_s (ms)	$\dot{P}_s$ (10^{-18} s s^{-1})	τ (10^9 yr)	B (10^8 G)	$\dot{E}$ (10^{34} erg cm^{-2}s^{-1})
J0613−0200[1]	06 13 43.97514(1.1)	−02 00 47.1737(4)	3.06	0.00882	5.50	1.66	1.3
J0614−3329	06 14 10.3478(3)	−33 29 54.118(3)	3.14	0.0175	2.84	2.38	2.2
J1231−1411[2]	12 31 11.3132(7)	−14 11 43.63(2)	3.68	0.0228	2.56	2.93	1.8
J2017+0603	20 17 22.7044(1)	+06 03 05.569(4)	2.89	0.0083	5.53	1.57	1.3

Notes. [1] $\mu_\alpha \cos(\delta) = 1.84 \pm 0.08$ mas yr^{-1}; $\mu_\delta = -10.6 \pm 0.2$ mas yr^{-1} (Verbiest et al. 2009).
[2] $\mu_\alpha \cos(\delta) = -100 \pm 2$ mas yr^{-1}; $\mu_\delta = -30 \pm 4$ mas yr^{-1} (Ransom et al. 2011).

Table 2. Orbital parameters (orbital period P_b and eccentricity e) of the pulsars listed in Table 1 as derived from the ATNF pulsar data base (second and third columns), together with the recomputed lower limits on the companion mass (M_C) inferred from the system mass function and assumed a pulsar mass $M_P = 1.4\,M_\odot$ and an orbital inclination $i = 90°$. Proposed classification of the companion star are given in the following column. References for the binary system mass function measurements and proposed classifications are given in the last column.

Pulsar	P_b (d)	e	M_C ($M_\odot$)	Class.	Refs.
J0613−0200	1.198	0.0000055	0.13	He WD	Verbiest et al. (2009)
J0614−3329	53.584	0.0001801	0.28	WD	Ransom et al. (2011)
J1231−1411	1.860	0.000004	0.19	WD	Ransom et al. (2011)
J2017+0603	2.198	0.0000005	0.18	He WD	Cognard et al. (2011)

pulsar evolution, including the different outcomes of the recycling process (e.g. Possenti & Burgay 2008; Possenti 2013), and investigate the possible evolutionary connections between different MSP types (e.g. Benvenuto, De Vito & Horvath 2014).

In all these types of studies, the optical identification of the MSP companion star plays a crucial role (e.g. Pallanca et al. 2012, 2013, 2014; Mucciarelli et al. 2013). In particular, optical observations, either via spectroscopy or broad-band photometry, are key to determine the star classification and physical parameters, such as surface temperature, surface gravity, and chemical composition of the atmosphere. This information then allow one to determine the age of the binary system (and that of the MSP independently of the measurements on P_s and $\dot{P}_s$) and track the system evolutionary history. Optical observations also allow one to find evidence for irradiation of the companion star through the identification of hot spots on the stellar surface. This can be a further tracer of the ablation process in BW and RB systems, after the more direct one which comes from the observation of eclipses of the radio signal as it propagates through the stellar wind from the irradiated MSP companion. For only ∼50 binary MSPs the companion star has been identified in the optical. Thus, for only about one third of the MSPs we know the optical characteristics of the companion star. In most cases, this is mainly due to the relatively large distances of these systems and the interstellar extinction in the Galactic plane, which hampers deep multiband optical observations. For the vast majority of non-eclipsing MSPs, the companion stars are found to be He WDs, although more cases of MSPs with CO WD companions have been found in the last few years (e.g. Mignani et al. 2014).

In this manuscript, we report on the search for the companion stars of four unidentified binary MSPs carried out using archival data from the Gemini South Telescope. We describe the MSPs sample and the observations in Section 2, while we present and discuss the results in Sections 3 and 4, respectively.

2 OBSERVATIONS

2.1 Target description

The names, measured radio coordinates, spin period (P_s), period derivative ($\dot{P}_s$), and inferred characteristics, spin-down age (τ), dipolar magnetic field (B), spin-down energy ($\dot{E}$), of the four MSPs studied in this work are summarized in Table 1.

Besides the radio band, all these MSPs have been detected as γ-ray pulsars by Fermi (Abdo et al. 2013). PSR J0614−3329, J1231−1411, and J2017+0603 were discovered during radio follow-ups of unidentified Fermi sources (Cognard et al. 2011; Ransom et al. 2011), whereas PSR J0613−0200 was discovered in radio by Manchester et al. (1996), prior to its detection as a γ-ray pulsar (Abdo et al. 2009).

All of them are also detected in the X rays by either *Suzaku*, *Chandra*, or *XMM–Newton* (see Abdo et al. 2013 and references therein). All these pulsars, with the exception of PSR J0614−3329, are in tight binary systems with orbital periods of ∼2 d or less and have almost circular orbits (Table 2), as expected from the outcome of the mass-accretion phase on to the MSP. The pulsar mass functions suggest low-mass companion stars with minimum masses $M_C \sim 0.13$–$0.3\,M_\odot$, after assuming a pulsar mass $M_P = 1.4\,M_\odot$ and an orbital inclination $i = 90°$ as indicative values. These assumptions are required since for none of these MSPs it was possible to measure the post-Keplerian parameters so far and for none of them evidence of radio eclipses has been found from the available observations (Verbiest et al. 2009; Cognard et al. 2011; Ransom et al. 2011).

Deep optical investigations with 8 m class telescopes have never been reported for these four MSPs. For both PSR J0613−0200 and PSR J1231−1411, optical observations were performed in 2010 January with the 2.4 m Isaac Newton Telescope (INT) at the La Palma Observatory (Canary Islands) soon after their detection as γ-ray pulsars (Collins, Shearer & Mignani 2011), whereas

Table 3. Observation log for the Gemini MSP observations.

PSR	Date yyyy-mm-dd	Filter	Number of exposures × Exposure time (s)	Airmass	seeing (arcsec)
J0613−0200	2010-11-06	*g*	1 × 30	1.14	0.77
		r	1 × 5+1 × 15+1 × 30	1.14–1.15	0.62
		i	1 × 5+1 × 30	1.5	0.61
	2010-12-29	*g*	7 × 30+7 × 60+7 × 120	1.14–1.18	0.94–1.20
		r	7 × 30+7 × 60+7 × 120	1.13–1.14	0.81–1.18
		i	7 × 30+7 × 60+7 × 120	1.14–1.17	0.63–1.00
J0614−3329	2010-09-08	*g*	10 × 240	1.1–1.58	0.72–1.18
		r	10 × 240	1.09–1.50	0.59–0.94
		i	8 × 240	1.12–1.45	0.69–0.83
	2010-09-14	*i*	1 × 30	1.02	0.85
		i	2 × 240	1.17–1.19	0.63
	2010-10-28	*g*	1 × 30	1.02	0.97
		r	1 × 30	1.02	0.88
J1231−1411	2010-12-31	*g*	1 × 30	1.25	1.15
		r	1 × 30	1.24	1.13
		i	1 × 30	1.24	1.03
	2011-01-03	*g*	6 × 240	1.33–1.37	0.87–1.05
		r	1 × 96+4 × 240	1.30–1.68	0.80–1.18
		i	4 × 240	1.39–1.57	0.76–0.81
	2011-01-29	*g*	6 × 240	1.04–1.08	0.84–1.21
		r	6 × 240	1.04–1.1	0.89–1.28
		i	6 × 240	1.04–1.1	0.82–1.13
J2017+0603	2010-08-05	*g*	1 × 92+1 × 200+8 × 240	1.24–1.35	0.85–1.15
		r	1 × 87+2 × 240	1.24	0.85
	2010-08-10	*r*	7 × 240	1.49–1.66	0.85–1.05
		i	10 × 240	1.33–1.47	0.60–0.89
	2010-08-31	*g*	1 × 30	1.24	0.95
		r	1 × 30	1.24	0.82
		i	1 × 30	1.24	0.80

for PSR J2017+0603, the only optical observations are those performed with the *Swift* Ultraviolet Optical Telescope (Cognard et al. 2011). In all cases, no candidate companion star to the MSP was detected.

2.2 Observation description

We downloaded broad-band images of the MSP fields from the public Gemini science archive.[2] Observations were taken between 2010 August 5 and 2011 January 29 with the Gemini South telescope on Cherro Pachon (Chile) under programme GS-2010B-Q-56. Observations were performed using the Gemini Multi-Object Spectrograph (GMOS). At the time of the observations, the camera was still mounting the original three-chip EEV CCD detector (2048 × 4068 pixels each). This had a combined (unvignetted) field-of-view of 5.5 arcmin × 5.5 arcmin, with gaps of 2.8 arcsec between each chip. The pixel scale was 0.1454 arcsec for a 2 × 2 binning. Observations were performed through the g_G0325 ($\lambda = 4750$ Å; $\Delta\lambda = 1540$ Å), r_G0326 ($\lambda = 6300$ Å; $\Delta\lambda = 1360$ Å), and i_G0327 ($\lambda = 7800$ Å; $\Delta\lambda = 1440$ Å) filters, very similar to the *g*', *r*', and *i*' used by the Sloan Digitised Sky Survey (SDSS; Fukugita et al. 1996).

For all targets the observation sequences in each filter consist of both short (typically 30 s) and long (240 s) exposures, with the former taken not to saturate bright stars in the field that can be used as secondary photometric reference frames. The exposure sequence was performed applying a dithering of a few arcseconds along the X-axis of the detector both to compensate for the gap between the CCD chips and account for the fringing affecting the i band. All targets were observed close to the zenith, with airmass mostly below 1.2, in dark time and mostly in photometric conditions. The complete observation log is reported in Table 3.

2.3 Data reduction and calibration

We reduced the GMOS images using the dedicated GMOS image reduction package available in the Image Reduction and Analysis Facility (IRAF) package.[3] After downloading the closest-in-time bias and sky flat-field frames from the Gemini science archive, we used the tasks `gbias` and `giflat` to process and combine the bias and flat-field frames, respectively. We then reduced the single science frames using the task `gireduce` for bias subtraction, overscan correction, image trimming, and flat-field normalization. These tasks work on a chip-by-chip basis and produce fully reduced images for each of the three GMOS CCDs. From the reduced science images, we produced a mosaic of the three GMOS CCDs using the task `gmosaic`. Finally, we aligned the reduced image mosaics to compensate for the dithering pattern applied to the exposure sequence and average-stacked the aligned images with the task `imcoadd` to filter out cosmic ray hits. Unfortunately, the dithering

[2] http://cadcwww.dao.nrc.ca/gsa/

[3] IRAF is distributed by the National Optical Astronomy Observatories, which are operated by the Association of Universities for Research in Astronomy, Inc., under cooperative agreement with the National Science Foundation.

pattern chosen for the observations happened not to be adequate to account for the effects of the fringing in the *i* band. For this reason, the *i*-band images obtained after frame stacking were still significantly affected by strong fringing. Applying the stacking to different image subgroups did not improve the results significantly. To remove the fringing, we followed the recipe suggested by the GMOS science operation team.[4] We downloaded from the Gemini science archive the template *i*-band fringe images closest in time to the epochs of our observations. Then, after flux normalization, we subtracted the fringe images from the single science images using the IRAF task `girmfringe`. Finally, we applied the same procedures as above to mosaic and stack the de-fringed *i*-band science images.

We computed the astrometry calibration of the optical images (both image mosaics and stacks) using the *wcstools*[5] suite of programs that automatically match the sky coordinates of stars selected from, e.g the Two Micron All Sky Survey (2MASS; Skrutskie et al. 2006) or the Guide Star Catalogue 2.3 (GSC2; Lasker et al. 2008) catalogues with their pixel coordinates computed by SExtractor (Bertin & Arnouts 1996). After iterating the matching process and applying a sigma-clipping selection to filter out obvious mismatches, high-proper motion stars, and false detections, a pixel-to-sky coordinate transformation was computed using a second-order polynomial function and we obtained, for the ground-based images mean residuals of ∼0.2 arcsec in the radial direction, using 50 bright, but non-saturated, 2MASS stars. To this value we added in quadrature the uncertainty $\sigma_{\rm tr} = 0.08$ arcsec of the image registration on the 2MASS reference frame. This is given by $\sigma_{\rm tr} = \sqrt{n/N_S}\sigma_{\rm S}$ (e.g. Lattanzi, Capetti & Macchetto 1997), where N_S is the number of stars used to compute the astrometric solution, $n = 5$ is the number of free parameters in the sky-to-image transformation model, $\sigma_{\rm S} \sim 0.2$ arcsec is the mean absolute position error of 2MASS for stars in the magnitude range $15.5 \leq K \leq 13$ (Skrutskie et al. 2006). After accounting for the 0.015 arcsec uncertainty on the link of 2MASS to the International Celestial Reference Frame (Skrutskie et al. 2006), we ended up with an overall accuracy of ∼0.2 arcsec on the absolute optical astrometry, i.e. comparable to the GMOS pixel size. Given the exquisite accuracy of MSP radio coordinates (Table 1) the uncertainty on the absolute astrometry calibration of the GMOS images obviously dominates the accuracy on the positional coincidence with a potential companion star.

We computed the photometry calibration using as a reference sets of secondary photometric standard stars extracted from the American Association of Variable Stars Observers (AAVSO) Photometric All-Sky Survey[6] (APASS), directly identified in each GMOS image of our MSP fields. We preferred to follow this approach rather than computing the photometry calibration using images of standard star fields (Smith et al. 2007) because there were no standard star observations taken on the same nights as the science observations. Moreover, a direct on-the-frame calibration obviously allows one to compensate for variations in the sky transparency during the night. The APASS photometric survey (Henden & Munari 2014) is calibrated on the SDSS photometric system and is, then, well suited to calibrate our GMOS *g*, *r*, *i*-band images. Like the SDSS, our photometry is, then, in the AB system (Oke 1974).

[4] http://www.gemini.edu/sciops/instruments/gmos/calibration/example-cal-data?q=node/10456
[5] www.harvard.edu/wcstools/
[6] http://www.aavso.org/apass

3 RESULTS

3.1 Astrometry

By using the astrometric solutions obtained as described in the section above, we checked all co-added science frames in each filter to look for objects detected at the computed radio position of our target MSPs (Table 1), which can be regarded as potential companion stars. For those pulsars which have a measured proper motion, i.e. PSR J0613−0200 (Verbiest et al. 2009) and PSR J1231−1411 (Ransom et al. 2011), we corrected the reference radio positions to the epoch of the Gemini observations.

For three pulsars (PSR J0614−3329, J1231−1411, J2017+0603), we clearly detected an object at the radio coordinates (see Fig. 1; top right to bottom left). In all cases the match was very good, with the object centroid almost perfectly coincident with the computed pulsar radio position. In particular, the measured angular separation between the MSP coordinates and those of its candidate companion was only ∼0.2–0.3 arcsec, i.e. comparable with the astrometric uncertainty of the GMOS images (∼0.2 arcsec; Section 2.3). Thus, in each case we considered the association with the MSP safe. To formally quantify the goodness of the associations between the MSPs and their candidate companions, we computed the probability that they are due to a chance coincidence. We computed this probability as $P = 1 - \exp(-\pi\rho r^2)$, where r is the measured angular separation between the MSP coordinates and those of its candidate companion (in arcsecond), and ρ is the density of stellar objects around the MSP positions per square arcsecond. Since, in principle, we do not know a priori the expected brightness range for the companion stars, we computed ρ without applying a selection in magnitude. For PSR J0614−3330 we computed a stellar density $\rho \sim 0.028$ and estimated a chance coincidence probability $P \sim 0.0035$, whereas for PSR J1231−1411 and PSR J2017+0603 we estimated $P \sim 0.004$ ($\rho \sim 0.014$) and $P \sim 0.010$ ($\rho \sim 0.038$), respectively. In all cases, the low chance coincidence probability would rule out spurious associations and would suggest that the candidate companions detected in the GMOS images are indeed associated with the MSPs.

For the fourth pulsar (PSR J0613−0200), the radio position fell slightly off-centre (∼2 arcsec to the north) with respect to the centroid of the closest object detected in the GMOS images (Fig. 1; top left), although it is still within its point spread function (PSF). However, the measured position offset is much larger than the 3σ uncertainty on our computed astrometric solution, with the uncertainty on the pulsar radio coordinates being negligible (Table 1). Thus, based on our astrometric solution, we infer that this object is not associated with PSR J0613−0200. Presumably, this object is the 'brightish star nearby' the pulsar, mentioned in table 1 of van Kerkwijk et al. (2005). This star was also identified by Mignani et al. (2014) in near-ultraviolet and optical images from the *Galaxy Evolution Explorer* (*GALEX*), the *XMM–Newton* Optical Monitor, and the *Swift* UltraViolet and Optical Telescope and ruled out as a candidate companion to the pulsar on the basis of its positional offset from the radio coordinates. The same star was also detected in images taken with the INT (Collins et al. 2011) but was considered unassociated to PSR J0613−0200 for the very same reason as above. The relatively high chance coincidence probability with the radio position also suggests that this star is unrelated to the pulsar. By assuming a radius $r \sim 2$ arcsec, i.e. equal to the angular separation between the star and the MSP radio coordinates, we obtain $P \sim 0.13$ ($\rho \sim 0.038$). To directly verify a possible, though

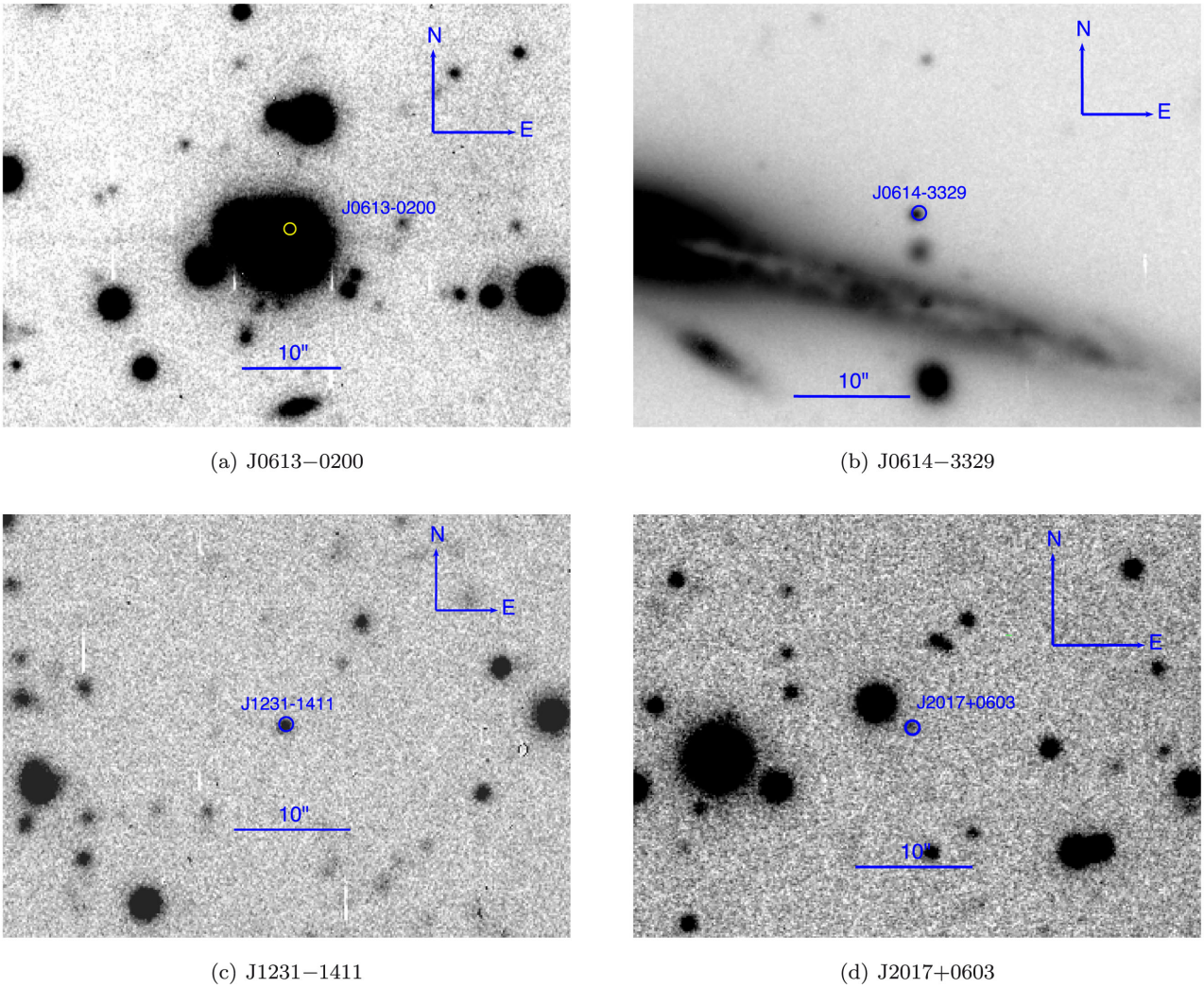

Figure 1. GMOS *r*-band images of the four MSP fields. The circles correspond to the computed MSP radio positions. Since the error on the radio coordinates is below 1 mas (see Table 1) the uncertainty on the computed radio position is dominated by the accuracy our astrometry calibration (0.2 arcsec; Section 3.2). The circle radius corresponds to three times such an uncertainty for a better visualization. For the other pulsars, the companion stars are marked by the ticks and labelled by the pulsar names. PSR J0614−3329 is located a few arcsec north of the disc of the bright galaxy ESO 365-1 (Lauberts & Valentijn 1989). All images have been obtained from the co-addition of all *r*-band science frames, apart from the PSR J0613−0200 one which has been obtained from the co-addition of short exposures only to avoid saturation of the bright star near the pulsar position.

unlikely, association between this star and the pulsar, we compared their measured proper motions. According to UCAC-4 (Zacharias et al. 2013), this star has a proper motion of $\mu_\alpha \cos(\delta) = 7.2 \pm 2.8$ mas yr^{-1} and $\mu_\delta = -4.6 \pm 2.9$ mas yr^{-1} in right ascension and declination, respectively, which is marginally consistent with the pulsar radio proper motion, $\mu_\alpha \cos(\delta) = 1.84 \pm 0.08$ mas yr^{-1} and $\mu_\delta = -10.6 \pm 0.2$ mas yr^{-1} (Verbiest et al. 2009). However, the UCAC-4 measurement is still below the 3σ significance so that the result of such a comparison is not conclusive. Thus, with all pieces of evidence pointing towards a chance coincidence, we conclude that the pulsar companion is most likely hidden in the PSF wings of this bright star.

3.2 Photometry

Since for all the target MSPs, the radio position is neatly located very close to the nominal GMOS pointing position at the centre of chip #2, we decided to use only images from the central chip for the following photometry analysis. This choice has the advantage of simplifying the procedure, with the tolerable cost of loosing the relatively small field of view of the two external chips, some of which are also affected by vignetting and partially occulted by the telescope autoguider. Moreover, adopting a smaller, but still significantly large field of view, has the advantage of reducing the effects of possible differential extinction along the line of sight due to, e.g. clumps in the interstellar medium.

We computed the photometry of the candidate MSP companion stars, as well as of the field stars, through a semi-automatic pipeline that makes use of the DAOPHOT II package (Stetson 1987, 1994) distributed as part of IRAF software environment. The pipeline consists of a set of scripts executing sequentially all the tasks needed to obtain a list of objects from a given image, with positions, magnitudes and errors. Namely, per each filter these tasks are: (i) obtain a master list of detected objects through the analysis of the master image, chosen as the co-added and exposure-map corrected science frame to maximize the detection signal-to-noise, (ii) obtain a reliable PSF

Table 4. Coordinates and multiband photometry for the candidate companions to the three MSPs (column one), as measured in the GMOS images. Magnitude values were computed from the mean of all the available measurements and are in the AB system (Oke 1974). Column four gives the angular separation Δr between the measured candidate companion and the MSP coordinates (Table 1).

PSR	α (hms)	δ ($^\circ\ '\ ''$)	Δr	g	r	i
J0614−3329	06 14 10.333	−33 29 54.19	0.19 arcsec	21.95 ± 0.05	21.70 ± 0.03	21.58 ± 0.03
J1231−1411	12 31 11.299	−14 11 43.39	0.31 arcsec	25.40 ± 0.23	23.95 ± 0.06	23.35 ± 0.11
J2017+0603	20 17 22.714	+06 03 05.82	0.29 arcsec	24.72 ± 0.28	24.06 ± 0.25	23.84 ± 0.17

model for all the images in the data set (single exposures and co-added science frames), (iii) perform the PSF-fitting photometry and aperture correction steps on both single exposures and co-added science frames to obtain magnitudes and errors of every object in the master list, (iv) apply the photometric calibration as described in the previous Section, (v) extract relevant data for the candidate MSP companion stars and some control objects selected among the closest neighbour stars, and, per each MSP field, (vi) perform a variability analysis of the different photometry measurements to spot possible flux variations of the candidate MSP companion stars. The only step of our photometry pipeline which is run manually is the selection of the objects for building the PSF model in step (ii), from the master list obtained from the master image. Once the starting sample has been selected, the actual PSF modelling is automatized. This procedure is a 'custom' version of what more specialized programs do (see e.g. ALLFRAME; Stetson 1994) and has been repeatedly tested in the past for similar works.

The final result of our photometry pipeline is a catalogue of positions (detector and celestial coordinates) and g, r, i flux measurements and errors for each MSP field and for each image (single exposures and co-added science frames) in our sample. Filter-to-filter matching was done in a trivial way because all the single-mosaic images are carefully registered on to the master. From this data set, we extracted time series for each candidate MSP companion (Section 3.3), identified from the astrometric matching with the radio positions, and built both colour–magnitude (CM) and colour–colour (CC) diagrams using mean magnitudes for both the candidate MSP companion stars and all stars detected around the MSP positions (Section 3.4).

Using the same approach as above, we computed a model PSF for all the PSR J0613−0200 images (single mosaics and co-added science frames). Then, we used it to subtract the star detected ∼2 arcsec from the pulsar radio position and search for possible objects hidden in its PSF wings. Unfortunately, the low signal-to-noise of the residuals after the subtraction of the star PSF did not allow us to find evidence of any excess of signal that could be associated with an object detected at the pulsar position. Thus, the actual companion to PSR J0613−0200 would be undetected in the GMOS images. Only higher spatial resolution observations, either with Adaptive Optics or with the *Hubble Space Telescope*, would make its detection possible. After subtracting the star PSF we estimated the upper limits on the flux of the PSR J0613−0200 companion star using the co-added science images as a reference. The 3σ upper limits computed at the pulsar radio position are $g = 25.0$, $r = 24.3$, and $i = 24.2$.

The companion stars to MSPs often feature optical variability along the orbital period of the binary system owing, for instance to tidal distortion of the star (e.g. Orosz & van Kerkwijk 2003) or the formation of hot spots on the star surface irradiated by the pulsar (e.g. Stappers et al. 2001). For this reason, we searched for possible evidence of variability in the light curves of the candidate companion stars to PSR J0614−3329, J1231−1411, J2017+0603, obtained from the multi-epoch GMOS photometry (Table 3).

As a criterion, we used only the photometric measurements obtained in those filters where the candidate companion star is brighter and is detected with the highest occurrence. For all MSP fields, these conditions are matched by the observations in the r filter. However, in all cases the reduced χ^2_r of the flux measurement distribution is quite low, with values of 0.18 (J0614−3330), 0.24 (J1231−1411), 0.06 (J2017+0603), and is compatible with random variations only.

Moreover, the small number of flux measurements, concentrated in short night fractions and repeated on two or three nights only, sometimes separated by up to a few weeks (see Table 3), largely undersample the known orbital periods. This is particularly true in the case of PSR J0614−3329 which has the longest orbital period ($P_b = 53.584$ d) among these three MSPs. Therefore, we cannot use the available multi-epoch flux information as a further piece of evidence to support the proposed identification between the MSPs and their candidate companion stars, so far only based on the very good positional coincidence with the pulsar radio coordinates.

3.3 Colour and magnitude analysis

Since no significant variations are seen in the objects' fluxes, we computed mean optical magnitudes in the g, r, and i filters for the candidate companion stars to PSR J0614−3329, J1231−1411, J2017+0603, after applying a σ clipping algorithm to filter out measurements more strongly affected by night-to-night fluctuations. The mean magnitudes of the MSP candidate companion stars are (Table 4): $g = 21.95 \pm 0.05$, $r = 21.70 \pm 0.03$, $i = 21.58 \pm 0.03$ (PSR J0614−3330), $g = 25.40 \pm 0.23$, $r = 23.95 \pm 0.06$, $i = 23.35 \pm 0.11$ (PSR J1231−1411), and $g = 24.72 \pm 0.28$, $r = 24.06 \pm 0.25$, $i = 23.84 \pm 0.17$ (PSR J2017+0603).

Incidentally, we note that the mean magnitudes of the star detected ∼2 arcsec from the computed radio position of PSR J0613−0200 (Fig. 1, top left) are: $g = 16.21 \pm 0.03$, $r = 15.54 \pm 0.03$, $i = 15.35 \pm 0.03$. This suggests that, at the pulsar parallactic distance of 1.25 ± 1.09 kpc (Verbiest et al. 2009), it would be an early main-sequence (MS) star, whereas the minimum companion star mass and the orbital parameters (Table 2) indicate a WD companion star to PSR J0613−0200, possibly an He WD (Lorimer et al. 1995). Moreover, MSPs with possible early MS companions are extremely rare, with PSR J1903+0327 being the only certified case so far (Freire et al. 2011). However, this MSP has a quite large orbital eccentricity ($e \sim 0.44$) and a long orbital period ($P_b = 95.17$ d), whereas PSR J0613−0200 is in an almost circular orbit with a short period (Table 2). This indicates that the two binary systems followed different evolutionary paths, hence with different companions, with PSR J1903+0327 probably being part of a triple system in origin with both the MS star and a WD (Freire et al. 2011). Therefore, the colour and magnitude analysis give a further piece of evidence that this star is unrelated to PSR J0613−0200.

An updated optical proper motion measurement for this star (see Section 3.1), together with radial velocity measurements from optical spectroscopy and/or multi-epoch optical photometry, would indisputably rule out its association with PSR J0613−0200.

For the other pulsars (PSR J0614−3329, J1231−1411, J2017+0603), we used the mean magnitudes of the candidate companion stars as a reference for their classification by analysing their locations in the observed (i.e. not corrected for the reddening) CM and CC diagrams. The observed CM and CC diagrams for the PSR J0614−3329, J1231−1411, and J2017+0603 fields are shown in Figs 2–4 (black filled circles). The locations of the candidate MSP companion stars are shown as blue filled circles with error bars. In order to reject outliers and include only high-confidence measurements, we plotted stars for which at least nine measurements per filter are available and with $\sigma < 0.08$.

As seen, also owing to the limited star sample, all the observed CM diagrams show a significant scatter that makes it difficult to recognize the characteristic stellar sequences. This scatter is mainly due to the different distance of the field stars and, to a lesser extent, to their different reddening. Moreover, since the coordinates of these MSPs points at different directions in the Galaxy they sample different stellar populations, i.e. from the Galactic disc, bulge, and halo. In the case of the PSR J2017+0603 field, however, the observed CM diagram shows evidence of a more defined stellar sequence. This suggests that most stars in the field of view belong to a more homogeneous stellar population, e.g. in an open cluster, although there is no known open cluster (or candidate) in the pulsar field. Alternatively, they might all be at a comparable distance from the Sun, as suggested by the line of sight to the pulsar field, which intercepts the Sagittarius spiral arm. For all pulsars, the location of the companion stars in the observed CC diagrams lies in most cases along, or close to the field stars, suggesting that the companions have no unusual colours. This might indicate that their colours would not be very much affected by an hypothetical irradiation from the MSP.

4 DISCUSSION

We compared the positions of the candidate companion stars in the observed CM and CC diagrams with stellar population models and template WD evolutionary tracks accounting for both the distance to the pulsar and the interstellar extinction along the line of sight. For none of the three MSPs there is a distance measurement based on the radio parallax. Thus, with all due caveats, we used as a reference the pulsar distance obtained from the dispersion measure (DM) and the Galactic free electron density n_e along the line of sight (NE2001; Cordes & Lazio 2002). We assumed a realistic uncertainty of ±20 per cent on the computed distance, as the authors recommended. This uncertainty is much larger than that derived from the errors on the DM but accounts, in most cases, for systematic effects related to the possible under/overestimation of the Galactic electron density in certain directions. For PSR J0614−3329, however, the uncertainty on the distance is probably much larger than 20 per cent since the line of sight to the pulsar is almost tangent to the Gum Nebula and the distance is likely half as estimated from the NE2001 model (Ransom et al. 2011). No direct measurement of the interstellar reddening along the line of sight is available for these pulsars. However, all of them have been detected in the X rays (Abdo et al. 2013). Therefore, as a reference, we estimated the reddening from the hydrogen column density $N_{\rm H}$ along the line of sight derived from the spectral fits to the X-ray spectra after applying the relation of Predehl & Schmitt (1995).

Table 5. Pulsar DM, obtained from the ATNF pulsar data base, and distance (D), inferred from the Galactic free electron density along the line of sight (Cordes & Lazio 2002), of the last three MSPs listed Table 1. For the distance, we assumed an uncertainty of ±20 per cent. The fourth and fifth columns give the hydrogen column density $N_{\rm H}$ derived from the fits to the MSP X-ray spectra (Abdo et al. 2013) and the Galactic extinction in the pulsar direction (A_V) derived from the $N_{\rm H}$ using the relation of Predehl & Schmitt (1995).

Pulsar	DM (pc cm^{-3})	D (kpc)	$N_{\rm H}$ (10^{20} cm^{-2})	A_V
J0614−3329[1]	37.049	1.88	$6.44^{+6.32}_{-2.01}$	$0.36^{+0.35}_{-0.12}$
J1231−1411	8.09	0.43	11.3 ± 5.1	0.63 ± 0.28
J2017+0603	23.918	1.57	10	0.56

Note. [1]The distance based on the DM might be overestimated by a factor of 2 or more (Ransom et al. 2011).

Then, we computed the extinction in the different filters using the extinction coefficients of Fitzpatrick (1999). We note that for both PSR J0614−3329 and J2017+0603 the X-ray spectrum is poorly constrained (see table 16 in Abdo et al. 2013), and so is the value of the column density $N_{\rm H}$. In particular, for the PSR J2017+0603 the $N_{\rm H}$ was set to the Galactic value in the pulsar direction and scaled for the pulsar distance (10^{21} cm^{-2}). We obtained a new estimate of the $N_{\rm H}$ from the pulsar DM by applying the linear fit between these two quantities computed by He, Ng & Kaspi (2013). For the DM towards PSR J2017+0603 (23.918 pc cm^{-3}) the fit yields $N_{\rm H} = 7.17^{+3.11}_{-2.15} \times 10^{20}$ cm^{-2}, where the errors are associated with the fit 90 per cent confidence interval. The $N_{\rm H}$ value computed from the He et al. (2013) fit is consistent with that reported in Abdo et al. (2013) and corresponds to $A_V = 0.40^{+0.17}_{-0.12}$, after applying the relation of Predehl & Schmitt (1995). The DM, inferred distance, $N_{\rm H}$, and estimated interstellar reddening along the line of sight for the three MSPs are summarized in Table 5.

First, we compared the observed CM and CC diagrams of the MSP fields with simulated stellar sequences computed from the Besançon models (Robin et al. 2004). We simulated these sequences for different stellar populations, i.e belonging to the MS, Red Giant Branch, or the WD branch, and for distance values up to 15 kpc. The simulated sequences for each MSP field are shown in the panels in Figs 2–4 as the grey-scale maps. In the CM diagrams, the dark grey regions correspond to distance values within ±20 per cent the assumed pulsar distance (see Table 5), whereas in the CC diagrams they correspond to magnitudes within ±0.05 the r-band magnitude of the pulsar candidate companion star. As seen, the spread in the simulated stellar sequences well reproduces the spread in the observed points, as expected for different stellar populations at different distances. Since the field stars are affected by an unknown interstellar extinction, and the simulations based on the Besançon models simply compute a reddening scaled proportionally to the assumed distance in a given direction, introducing a reddening correction in our simulations might bias a direct comparison between the observed and the simulated stellar sequences. Therefore, for simplicity, in all cases we simulated the stellar sequences assuming a null reddening. Each panel also shows the reddening vector corresponding to the $E(B-V)$ estimated from the $N_{\rm H}$ measured along the line of sight to each MSP (Table 5) and computed using the extinction coefficients of Fitzpatrick (1999). Then, we used the reddening vectors as a reference to trace the extinction-corrected locations of the observed points for the MSP companion stars (blue points) along the simulated stellar sequences.

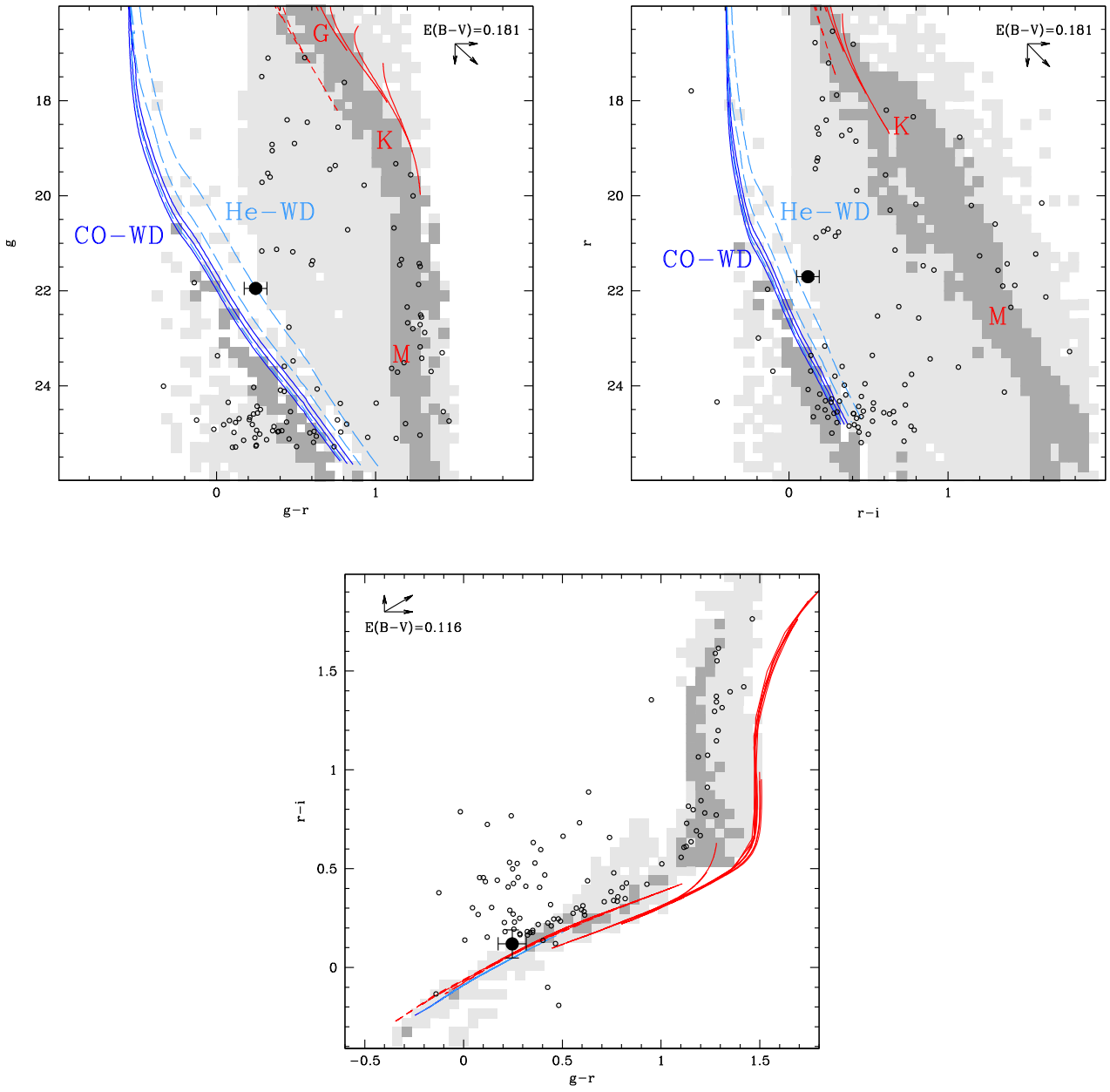

Figure 2. Observed CM (top row) and CC (bottom row) diagrams for all the stars in a ∼2.0 arcmin × 5.5 arcmin sky region around the PSR J0614−3329 position (filled black circles). The candidate companion star to the pulsar is marked by the black filled circle. Stellar sequences simulated from the Besançon models for different values of distance are shown in light and dark grey. In the CM diagrams the dark grey regions correspond to distance values within ±20 per cent the assumed pulsar distance (see Table 5), whereas in the CC diagram they correspond to magnitudes within ±0.05 the *r*-band magnitude of the pulsar candidate companion star. Theoretical evolutionary tracks for both He WDs (0.2, 0.25, 0.35 $M_{\odot}$; light blue dashed lines) and low-mass CO WDs (0.35, 0.4, 0.45 $M_{\odot}$; dark blue solid lines) are represented, computed from the models of Panei et al. (2007) for an age up to 4.8 Gyr and for the nominal values of the MSP distance. Masses increase from right to left. Evolutionary tracks for MS stars for both $Z = 0.02$ (red solid lines) and $Z = 0.0001$ (red dashed lines) are also shown for different mass ranges (0.5–1 $M_{\odot}$, with steps of 0.1 $M_{\odot}$) and for the nominal MSP distance. Masses decrease from top to bottom. Only in this case we assumed a distance value half of that obtained from the DM (see discussion in Ransom et al. 2011). Both the simulated stellar sequences from the Besançon models and the WD and MS evolutionary tracks were plotted assuming a null reddening. Reddening vectors are shown on the top of each panel. The lengths of the vectors correspond to the $E(B-V)$ estimated from the hydrogen column density inferred from the fits to the MSP X-ray spectrum. We used the extinction coefficients of Fitzpatrick (1999).

As seen, for all the three MSPs the location of the candidate counterpart in the diagrams falls off the region of the simulated MS and close to that of the simulated WD sequence. This is consistent with a WD identification for all the candidate companion stars, as proposed in the literature (Cognard et al. 2011; Ransom et al. 2011). We note that non-degenerate companion stars as those in BW or RB systems would be much closer than observed to the late MS (see e.g. Pallanca et al. 2012). Moreover, the minimum mass of the companion stars and the orbital period of the binary system (Table 2) would rule out that these MSPs are BWs or RBs

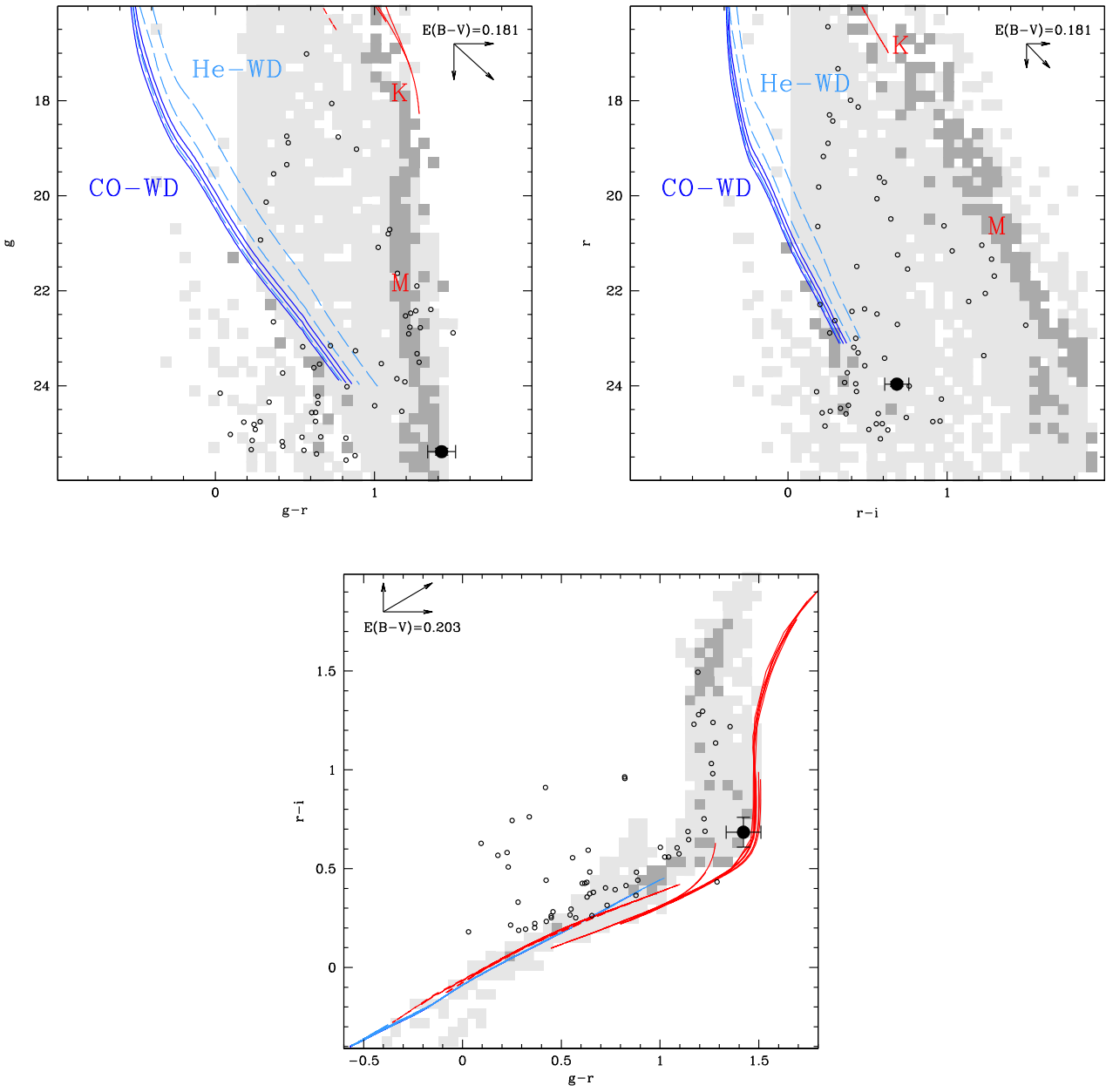

Figure 3. Same as Fig. 2 but for the PSR J1231−1411 field.

(see e.g. fig. 1 in Roberts 2013). Indeed, the minimum companion masses are larger than those of BW companions, whereas the orbital periods are larger than those of known RB binary systems, which have all orbital periods shorter than 1 d. The latter case is especially true for PSR J0614-3329 which has an orbital period of 53.584 d.

In order to better determine the WD characteristics, obtain a first tentative estimate of their mass and an independent estimate of the age of the binary system, we used the model evolutionary tracks of Panei et al. (2007), which are computed for both He and low-mass CO WD types, and different WD masses. In particular, these tracks are quite suited to our goal since the assumed range of WD masses is close to the minimum mass of the companions inferred from the mass function of the binary systems (Table 2). These tracks[7] also predict magnitude values for both WD types in the same photometric system as used by the GMOS observations, i.e. the SDSS one (Fukugita et al. 1996).

As an example, Figs 2–4 show the evolutionary tracks simulated for both an He WD (light blue) and a low-mass CO WD (dark blue).

The evolutionary tracks span an age range up to 4.8 Gyr, where the age limit corresponds to that of the available model (Panei et al. 2007), and different masses.

As a reference, we also plotted the evolutionary tracks of MS stars for both $Z = 0.02$ (red solid lines) and $Z = 0.0001$ (red dashed

[7] http://fcaglp.fcaglp.unlp.edu.ar/evolgroup/TRACKS/tracks_heliumcore.html

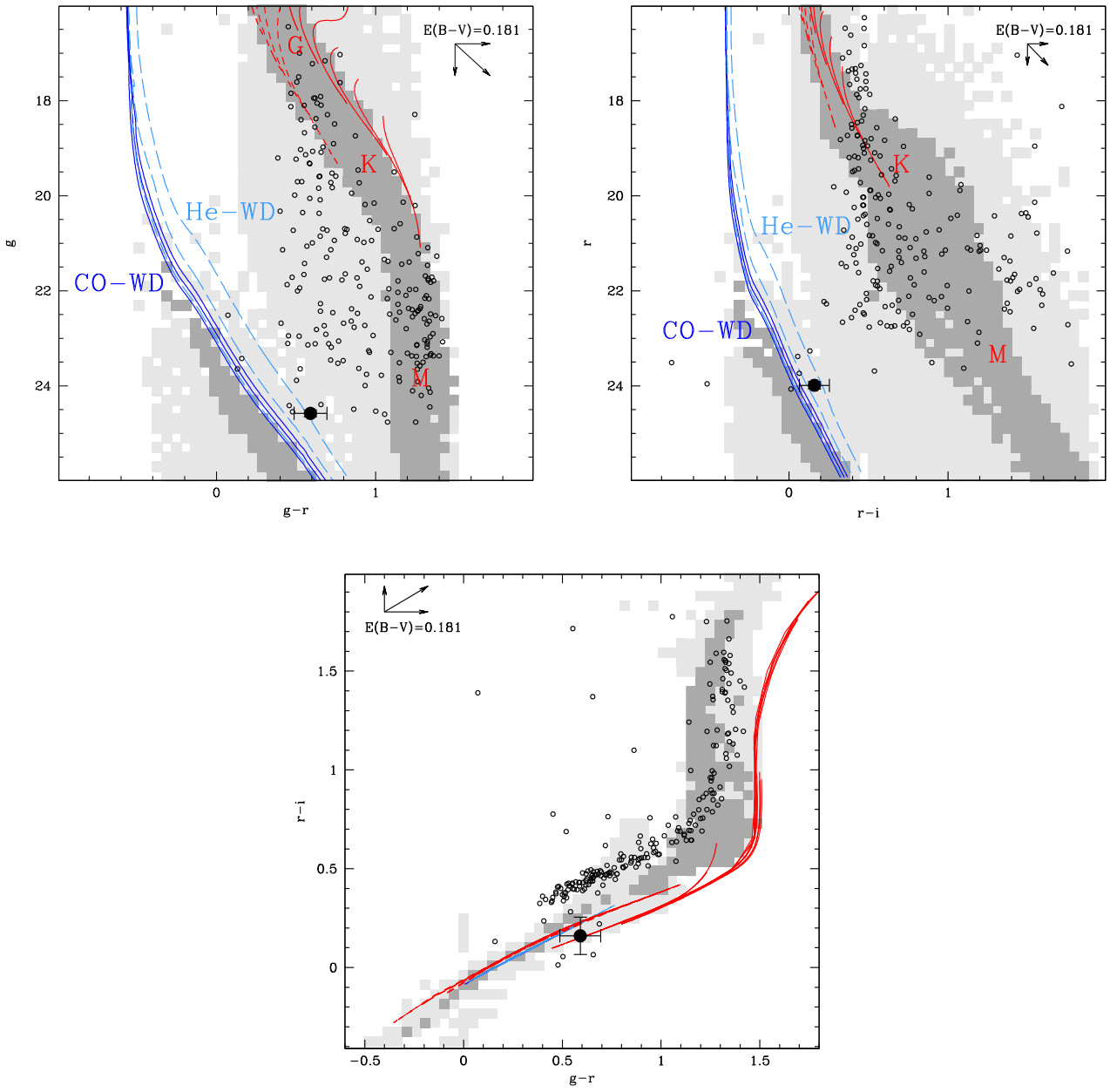

Figure 4. Same as Fig. 2 but for the PSR J2017+0603 field.

lines) and for different mass ranges (0.5–1 $M_{\odot}$, with steps of 0.1 $M_{\odot}$). In each figure, the lines correspond to the nominal value of the MSP distance (Table 5).

Following Ransom et al. (2011), for PSR J0614−3329 we assumed a distance value half of that obtained from the DM and the NE2001 model. As done for the simulated stellar sequences computed from the Besançon models, we plotted the simulated WD and MS evolutionary tracks assuming a null extinction, for simplicity. As seen, for both PSR J0614−3329 and J2017+0603 the location of the candidate companion star in the CM and CC diagrams seems to be more compatible with the simulated evolutionary tracks for an He WD (light blue lines), than for a low-mass CO WD (dark blue lines). The difference between the He and CO WD evolutionary tracks is more evident for PSR J0614−3329, whereas for J2017+0603 the *r*–*i* colour is partially compatible with both WD types. The location of the candidate companion star to PSR J1231−1411 in the CM and CC diagrams does not overlap with any of the evolutionary tracks, although it seems to be consistent with the extrapolation of the He WD evolutionary tracks. Since these are computed for a maximum age of 4.8 Gyr, it means that the companion star must be significantly older than those of PSR J0614−3329 and J2017+0603.

To summarize, our qualitative analysis of the CM and CC diagrams seems to suggest that the candidate companions to these three MSPs are more probably He WD than low-mass CO WDs. However, owing to the uncertainties in extrapolating the evolutionary tracks for ages above 4.8 Gyr, we regard the possible identification of the PSR J1231−1411 companion as an He WD as more uncertain than in the other cases. In addition, it should be considered that CO WDs tracks tend to separate and spread out at low effective

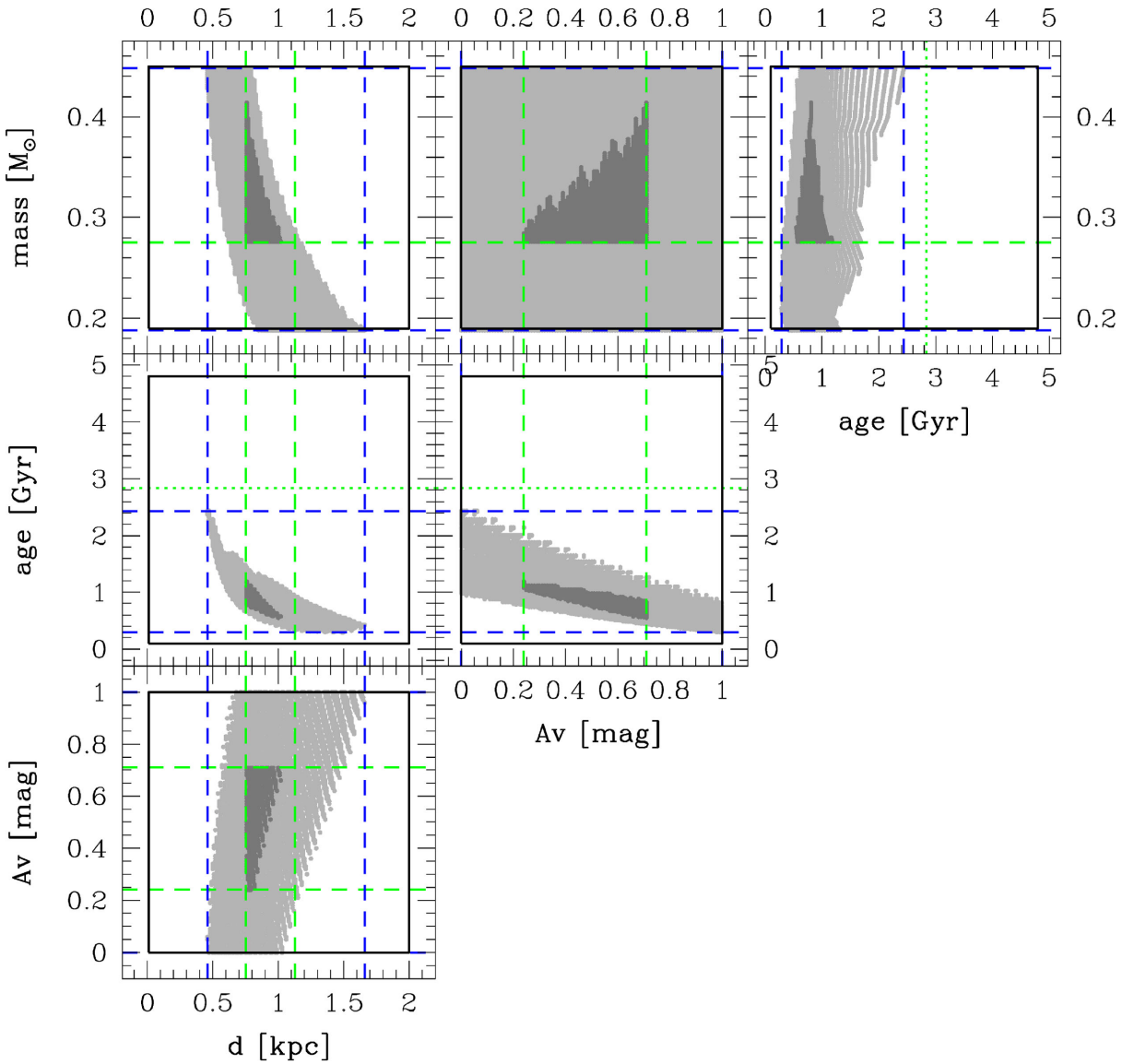

Figure 5. Pair combinations of the four parameters which we used to fit the observed magnitudes and colours of the candidate companion star to PSR J0614−3329 with mode evolutionary tracks (Panei et al. 2007). This plot refers to the case of an He WD. The thick black lines mark the investigated region in each plane of the parameter space. The light grey regions mark, for each pair of parameters, the allowed parameter configurations which reproduce the observed optical properties of the candidate companion stars (magnitudes, colours). The extreme of these regions projected on each axis are marked by the blue lines, while the green dashed lines mark the parameter range constrained by the radio and X-ray measurements. Although the radio/X-ray constraints of each parameter pair seem to be more stringent than the optical ones, imposing that all conditions are simultaneously satisfied shrinks the allowed parameter configurations to the dark grey regions. The dotted green line corresponds to the pulsar spin-down age.

temperatures due to different atmospheric compositions. An example of this can be seen in Bergeron et al. (2011) and references therein.

We tried to verify more quantitatively a possible association with either of the two types for different values of the WD mass and age, and for different values of the distance and reddening. To this aim, we systematically investigated all possible combinations in a four-dimensional parameter grid and selected only those for which the optical magnitudes and colours predicted by the model evolutionary tracks for He or low-mass CO WDs were found to be consistent with the observed ones, within the measured photometry uncertainties. We considered the case of He WDs first. Figs 5–7 show the allowed combinations for each of the selected pairs of parameters for the He WD case. For visualization purposes, in each panel the regions corresponding to the allowed parameter combinations are plotted in light grey. The discontinuity in the grey regions noticed in some panels are purely an effect of the parameter quantization. The black thick lines in each panel mark the investigated parameter range. We considered a range of values around those expected from radio and optical observations, with a generous tolerance to account for the associated uncertainties. In particular, we considered a range of distances $0.01 < d < 2$ kpc (0.01 kpc steps) and $0 < A_V < 1$ (0.01 mag steps). For the companion mass, we considered the range $0.188\,M_\odot < M_C < 0.488\,M_\odot$ (0.002 $M_\odot$ steps), which is that of the model evolutionary track for He WDs (Panei et al. 2007). We derived WD tracks for intermediate mass values from a linear interpolation between the tracks corresponding to the available mass values. Finally, for the age we considered a range of values obtained

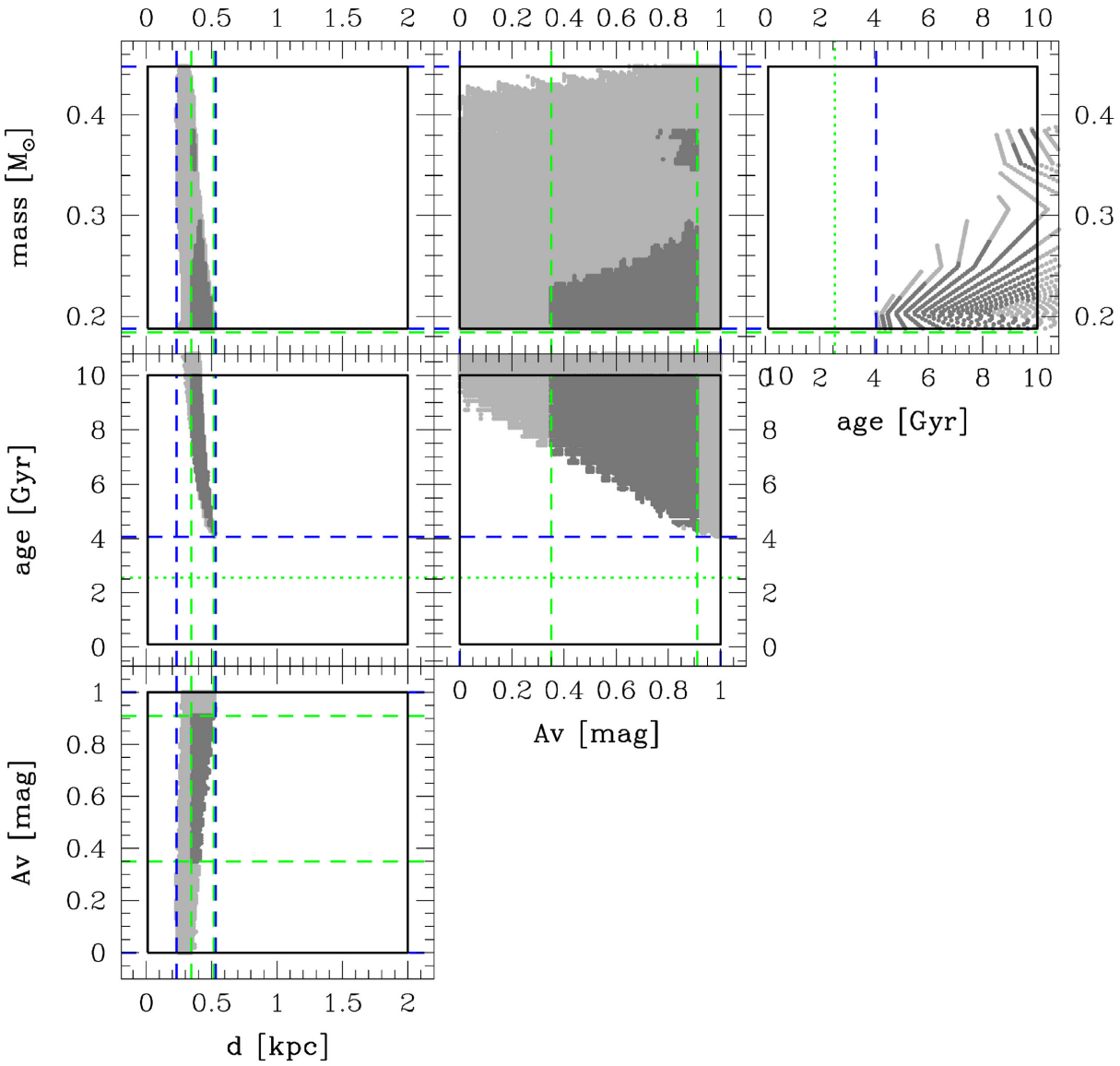

Figure 6. Same as Fig. 5 but for PSR J1231−1411.

from the computed WD tracks, for a given value of WD mass and extinction, with steps of 0.1 mag in the *r*-band magnitude. We remind that for PSR J1231−1411 the comparison with the WD tracks is based on their extrapolation for ages above 4.8 Gyr and is obviously more uncertain than for the other two MSPs.

Possible parameter ranges, purely imposed by the observed colours and magnitudes of the companion star, are represented by the blue dashed lines intercepting tangentially the light grey regions in each panel in Figs 5–7. Note that in some panels the black thick lines and the dashed blue lines coincide. This corresponds to those cases where the uncertainty on our photometry is not sufficiently small to better constrain the parameter value. Then, we considered, with the due caveats, the limits imposed by the radio observations on the MSP parameters, such as the lower limit on the companion mass M_C (Table 2) and the pulsar distance (Table 5), and the limits imposed by the X-ray observations, such as the N_H and the inferred interstellar extinction (Table 5). We did not apply any limit to the WD age based on the pulsar spin-down age because of the well-known difficulties in determining a reliable uncertainty range for this value other than that the formal error derived from the measured P_s and $\dot{P}_s$, of course (e.g. Lorimer & Kramer 2005). Finally, we selected only the configurations for which all conditions imposed to all pair of parameters by the limits derived from optical, radio, and X-ray observations were simultaneously satisfied. The selected parameter configurations are represented by the dark grey regions in the panels in Figs 5–7. For PSR J1231−1411, the obtained age range originally spanned values larger than the age of the Universe. Therefore, we imposed that the WD age is smaller than an arbitrary value, which we set to 10 Gyr. The plots in Fig. 6 were updated accordingly.

We repeated the same analysis as above for the low-mass CO WD case. We assumed the same range of distance and extinction values as in the previous case and the range of companion star masses ($0.351\,M_\odot < M_C < 0.448\,M_\odot$) from the model evolutionary tracks for low-mass CO WDs (Panei et al. 2007). We computed the age range exactly as in the previous case. We found that all the allowed configurations (not shown here) imply companion masses of $\lesssim$0.4 $M_\odot$ (PSR J0614−3329, PSR J2017+0603) and $\lesssim$0.36

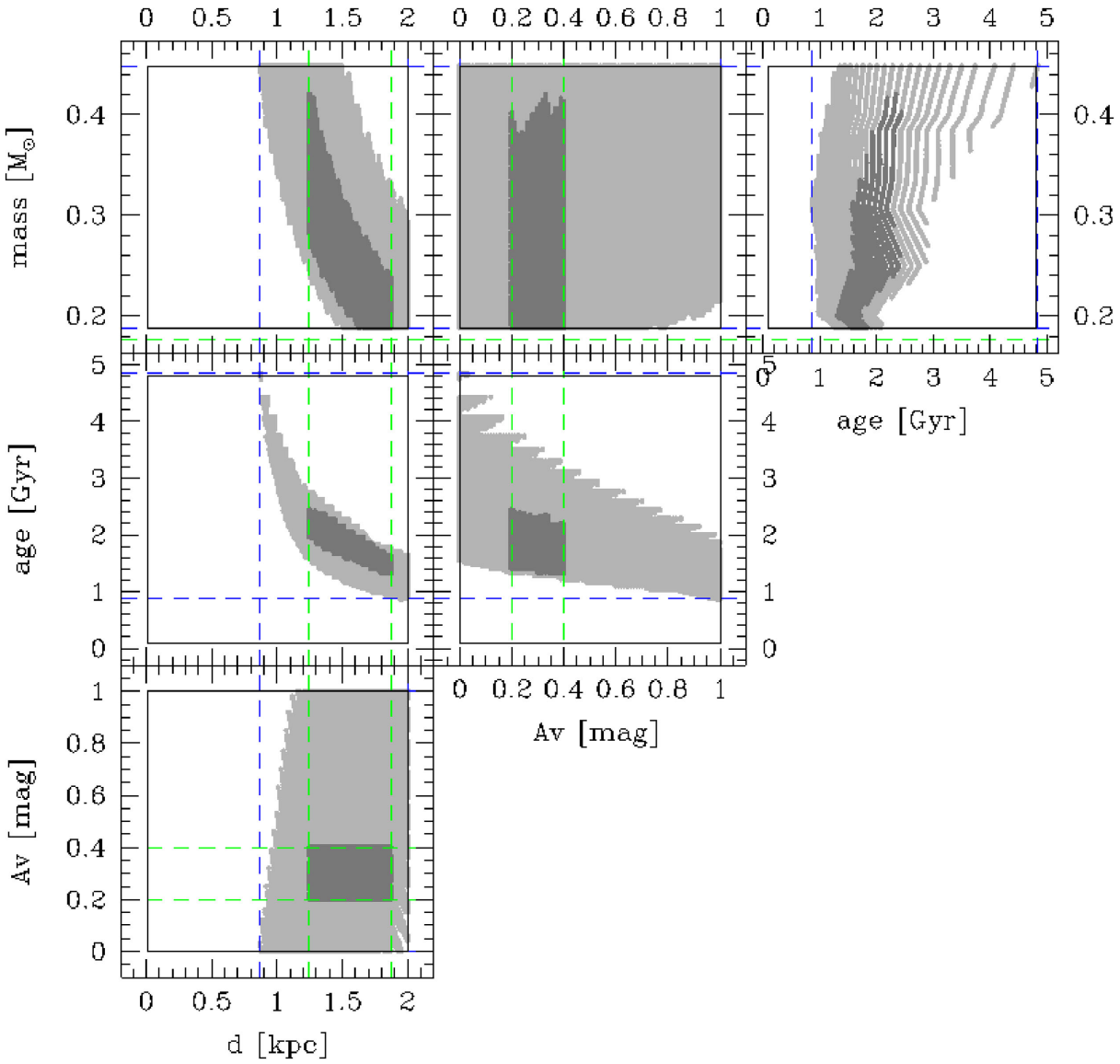

Figure 7. Same as Fig. 5 but for PSR J2017+0603.

$M_\odot$ (PSR J1231−1411), i.e. at the low end of the mass range even for low-mass CO WDs. This would make a CO WD companion for the three MSPs somewhat less likely, although this possibility can be firmly ruled out only with a better characterization of the star spectra through follow-up spectroscopy observations. Our results are in line with the qualitative analysis of the CM and CC diagrams (Figs 2–4) and the possibility that the candidate companion stars of the three MSPs are He WDs.

The derived parameter ranges for the three MSP companions are summarized in Table 6, for the He WD case. In the first half, we report the ranges of WD age, mass, distance, and extinction obtained from the above analysis (Figs 5–7), whereas in the second half we report the values of the WD surface temperature, luminosity, and surface gravity extracted from the model, which correspond to the obtained age and mass ranges. Unfortunately, for both PSR J1231−1411 and PSR J2017+0603, which are the MSPs with the faintest companion stars (Table 4), the photometry errors were so large that several sets of parameters were able to fit the observed optical magnitudes and colours, although the parameter degeneracy has decreased (see Figs 6 and 7). On the other hand, the smaller photometry errors for PSR J0614−3329 made it easier to find possible ranges for the different parameters. We note that our results are influenced by the model uncertainties, including the characterization of the WD atmosphere and composition, and by the overall uncertainties on the predicted magnitudes, which are more difficult to quantify than the photometry errors on the observed magnitudes, by some arbitrary assumptions on the parameter uncertainties, such as on the pulsar distance, and by the uncertainty on the extrapolated parameters, such as the interstellar extinction. Therefore, the inferred ranges for the WD parameters should not be taken rigidly but only as indicative. This is particularly true in the case of PSR J1231−1411 (see above). Spectroscopy observations and multiband light curves will be needed to obtain a better characterization of the companion star properties and pave the way to a more robust comparison with stellar models.

For all our pulsars, we found a possible range of values for the companion mass M_C. As it has already been observed, a correlation has been found between the orbital period P_b and the companion

Table 6. Parameters for the candidate companion stars to the MSPs obtained from Figs 5–7 and the comparison with He WD model evolutionary tracks (Panei et al. 2007). Top section: derived ranges for the mass and age of the companion star (M_C) to the MSP, distance (D) and interstellar extinction along the line of sight (A_V). These ranges basically correspond to the outermost values of the dark grey regions of Figs 5, 6, and 7. In case of PSR J1231−1411, these ranges were obtained by imposing that the WD age is <10 Gyr. Bottom section: ranges of WD surface temperature T, luminosity L, and gravity $\log g$ corresponding to the above mass and age ranges.

	PSR J0614−3329	PSR J1231−1411	PSR J2017+0603
M_C [$M_\odot$]	0.276–0.414	0.188–0.384	0.188–0.42
Age [Gyr]	0.55–1.18	4.30–10	1.31–2.44
D [kpc]	0.76–1.02	0.35–0.51	1.25–1.87
A_V [mag]	0.24–0.71	0.35–0.91	0.2–0.4
T [K]	7237–9666	2652–4009	5412–6437
$\log[L/L_\odot]$	[−2.898, −2.386]	[−4.549, −3.920]	[−3.346, −3.014]
$\log g$	7.107–7.572	6.973–7.603	6.778–7.625

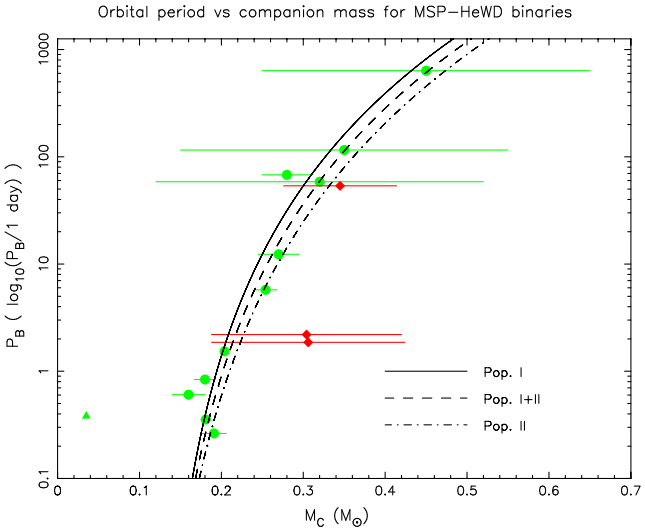

Figure 8. Orbital period P_b versus companion mass M_C for MSP-He-WD binaries (green filled circles; updated from Corongiu et al. 2012). Error bars correspond to 1σ uncertainties in the masses. If not visible, their size is smaller than the symbol. The red diamonds correspond to the three MSPs for which we identified the companion stars: PSR J0614−3329, PSR J2017+0603, and PSR J1231−1411 (top to bottom). The black filled triangle corresponds to the BW PSR B1957+20. The solid, dashed, and dot–dashed lines are the tracks corresponding to the theoretical correlation found by Tauris & Savonije (1999).

mass M_C for binary systems hosting a MSP and an He WD (see e.g. Corongiu et al. 2012 and references therein). Such a correlation was theoretically found by Tauris & Savonije (1999) and has been confirmed by the mass measurements of the companion star in about a dozen of such systems. The predictions by Tauris & Savonije (1999) indicate, for the three MSP binary systems discussed here, a value for the companion mass that would lie in the range that we obtained from our estimates (Table 6). This is seen in Fig. 8 (updated from Corongiu et al. 2012), where we show the P_b–M_C plot for all MSPs with an He WD companion of measured mass together with the estimated masses for the companion stars to PSR J0614−3329, PSR J1231−1411, and PSR J2017+0603.

For both PSR J0614−3329 and PSR J2017+0603, the inferred age estimate for the WD companion would be smaller than the pulsar spin-down age τ by a factor of ∼2.4–5 (Table 1). On the other hand, in the case of PSR J1231−1411 the minimum age of the WD companion obtained from our analysis would be ∼ 70 per cent greater than the pulsar spin-down age. However, it has been shown (e.g. Tauris 2012) that spin-down ages are not reliable age estimators for MSPs. Therefore, we must take this discrepancy with the due care. Since for PSR J1231−1411, we had to impose an arbitrary upper limit to the age of the companion star, only for PSR J0614−3329 and PSR J2017+0603 we could obtain a first estimate of the cooling age of the WD, which would be of the order of about 0.8 and 1.7 Gyr, respectively.

For PSR J0614−3329, the derived range for the pulsar distance purely imposed by the observed colour and magnitude of the companion star (blue lines in Fig. 5), would confirm that the distance to the pulsar is indeed about half the value inferred from the DM and the NE2011 model (Table 5), as suggested by Ransom et al. (2011). On the contrary, the corresponding range for PSR J1231−1411 would indicate that the pulsar distance cannot be much larger than the value obtained from the DM, whereas its high Galactic latitude ($b \sim 48^\circ$) and the low value of the DM (8.09 pc cm^{-3}) might have suggested that such a value is underestimated by a factor of 2 (Gaensler et al. 2008; Chatterjee et al. 2009).

We used the mass and age ranges of the WD companions derived above to select the associated ranges of the star surface temperature T, luminosity and surface gravity $\log g$ (second half of Table 6) from the He WD model evolutionary tracks (Panei et al. 2007). As seen, the WD companion star to PSR J1231−1411 would stand out for its lower temperature ($T \sim$ 2600–4000 K), definitely on the lower end of the WD temperature distribution, and lower luminosity ($\log[L/L_\odot] \approx -4$) with respect to the other MSP companions. The inferred lower temperature was also anticipated by the observed reddish colour of the star (Fig. 3). Thus, the WD companion to PSR J1231−1411 would be one of the coolest WDs known so far. If confirmed, this result would be exceptional but not unheard of. We note that a very low temperature WD companion ($T <$ 3000 K) has been likely identified also in the MSP binary system PSR J2222−0137 (Kaplan et al. 2014). On the other hand, both the WD companion stars to PSR J0614−3329 and PSR J2017+0603 would be hotter, with temperatures more compatible with the values expected for a WD ($T \sim$ 7000–10 000 K), and are more luminous ($\log[L/L_\odot] \approx -3$).

5 SUMMARY AND CONCLUSIONS

Using the Gemini South telescope, we identified the likely companion stars to three MSPs (PSR J0614−3329, J1231−1411, and

J2017+0603). For a fourth pulsar (PSR J0613−0200), the identification of the companion star was hampered by the presence of a bright star ($g = 16 \pm 0.03$) at ∼2 arcsec from the pulsar radio position. We ruled out with a reasonable confidence that this star is a candidate companion to the pulsar. The companion stars of the other three MSPs can be possibly identified as He WDs on the basis of multiband photometry and comparison with simulated stellar models (Panei et al. 2007). For PSR J1231−1411, the identification is somewhat more uncertain owing to the more ambiguous match with the evolutionary tracks. If these identifications were confirmed, they would prove that He WDs tend to be the most common companions to non-eclipsing MSPs, as suggested by the number of MSP companions which have been identified in the optical so far. For PSR J0614−3329, J1231−1411, and J2017+0603, we derive possible ranges for the WD mass, age, surface temperature, luminosity, and gravity (see Table 6) within the ranges predicted by the assumed He WD models and optical/radio observations. For none of these three MSPs we could look for flux modulations at the orbital period of the binary system, owing to the sparse data points and the uneven time coverage of the orbital period provided by the Gemini observations. Future variability studies of the companion star fluxes through optical photometry, together with the measurements of the radial velocity curves through optical spectroscopy with 8 m class telescopes, will firmly prove the proposed associations with the MSPs, currently based upon a very good positional coincidence with the radio coordinates and the colours of the candidate companions stars. Optical spectroscopy would also be crucial to verify our tentative classification of the MSP companion stars as He WDs, so far only based upon optical broad-band photometry in three bands, obtain more robust measurements of their stellar parameters, such as the mass, surface temperature, and gravity, and provide information on the atmosphere composition.

ACKNOWLEDGEMENTS

We thank the anonymous referee for his/her constructive comments to the manuscript. We are grateful to Dr. Achille Nucita (University of Salento, Lecce, Italy) for his advice in the variability analysis. The research leading to these results has received funding from the European Commission Seventh Framework Programme (FP7/2007-2013) under grant agreement no. 267251. This research is part of the project COSMIC-LAB funded by the European Research Council (under contract ERC-2010-AdG-267675). This research is based on observations obtained at the Gemini Observatory, which is operated by the Association of Universities for Research in Astronomy, Inc., under a cooperative agreement with the NSF on behalf of the Gemini partnership: the National Science Foundation (United States), the National Research Council (Canada), CONICYT (Chile), the Australian Research Council (Australia), Ministério da Ciência, Tecnologia e Inovação (Brazil) and Ministerio de Ciencia, Tecnología e Innovación Productiva (Argentina). This research has made use of the APASS data base, located at the AAVSO web site. Funding for APASS has been provided by the Robert Martin Ayers Sciences Fund.

REFERENCES

Abdo A. A. et al., 2009, Science, 325, 848
Abdo A. A. et al., 2013, ApJS, 208, 17
Alpar M. A., Cheng A. F., Ruderman M. A., Shaham J., 1982, Nature, 300, 728
Benvenuto O. G., De Vito M. A., Horvath J. E., 2014, ApJ, 786, L7
Bergeron P. et al., 2011, ApJ, 737, 28
Bertin E., Arnouts S., 1996, A&AS, 117, 393
Bhattacharya D., van den Heuvel E. P. J., 1991, Phys. Rep., 203, 1
Chatterjee S. et al., 2009, ApJ, 698, 250
Cognard I. et al., 2011, ApJ, 732, 47
Collins S., Shearer A., Mignani R. P., 2011, in Burgay M., D'Amico N., Esposito P., Pellizzoni A., Possenti A., eds, AIP Conf. Proc. Vol. 1357, Radio pulsars: an Astrophysical Key to Unlock the Secretes of the Universe. Am. Inst. Phys., New York, p. 310
Cordes J. M., Lazio T. J. W., 2002, preprint (astro-ph/0207156)
Corongiu A. et al., 2012, ApJ, 760, 100
Fitzpatrick E. L., 1999, PASP, 111, 63
Freire P. C. C. et al., 2011, MNRAS, 412, 2763
Fukugita M., Ichikawa T., Gunn J. E., Doi M., Shimasaku K., Schneider D. P., 1996, AJ, 111, 1748
Gaensler B. M., Madsen G. J., Chatterjee S., Mao S. A., 2008, PASA, 25, 184
He C., Ng C.-Y., Kaspi V. M., 2013, ApJ, 768, 64
Henden A., Munari U., 2014, Contrib. Astron. Obs. Skalnaté Pleso, 43, 518
Kaplan D. L. et al., 2014, ApJ, 789, 119
Lasker B. M. et al., 2008, AJ, 136, 735
Lattanzi M. G., Capetti A., Macchetto F. D., 1997, A&A, 318, 997
Lauberts A., Valentijn E. A., 1989, The Surface Photometry Catalogue of the ESO-Uppsala Galaxies. European Southern Observatory, Garching
Lorimer D. R., Kramer M., 2005, Handbook of Pulsar Astronomy. Cambridge Univ. Press, Cambridge
Lorimer D. R. et al., 1995, ApJ, 439, 933
Lyne A. G., Brinklow A., Middleditch J., Kulkarni S. R., Backer D. C., 1987, Nature, 328, 399
Manchester R. N. et al., 1996, MNRAS, 279, 1235
Manchester R. N., Hobbs G. B., Teoh A., Hobbs M., 2005, AJ, 129, 1993
Mignani R. P. et al., 2014, MNRAS, 443, 2223
Mucciarelli A., Salaris M., Lanzoni B., Pallanca C., Dalessandro E., Ferraro F. R., 2013, ApJ, 772, L27
Oke J. B., 1974, ApJS, 27, 21
Orosz J. A., van Kerkwijk M. H., 2003, A&A, 397, 237
Pallanca C., Mignani R. P., Dalessandro E., Ferraro F. R., Lanzoni B., Possenti A., Burgay M., Sabbi E., 2012, ApJ, 755, 180
Pallanca C., Lanzoni B., Ferraro F. R., Dalessandro E., Possenti A., Salaris M., Burgay M., 2013, ApJ, 773, 127
Pallanca C., Ransom S. M., Ferraro F. R., Dalessandro E., Lanzoni B., Hessels J. W. T., Stairs I., Freire P. C. C., 2014, ApJ, 795, 29
Panei J. A., Althaus L. G., Chen X., Han Z., 2007, MNRAS, 382, 779
Possenti A., 2013, in van Leeuwen J., ed., Proc. IAU Symp. 291, Neutron Stars and Pulsars: Challenges and Opportunities after 80 years. Cambridge Univ. Press, Cambridge, p. 121
Possenti A., Burgay M., 2008, in Wijnands R., Altamirano D., Soleri P., Degenaar N., Rea N., Casella P., Patruno A., Linares M., eds, AIP Conf. Proc. Vol. 1068, A decade of accreting millisecond X-ray pulsars. Am. Inst. Phys., New York, p. 17
Predehl P., Schmitt J. H. M. M., 1995, A&A, 293, 889
Ransom S. M. et al., 2011, ApJ, 727, L16
Roberts M. S. E., 2013, in van Leeuwen J., ed., Proc. IAU Symp. 291, Neutron Stars and Pulsars: Challenges and Opportunities after 80 years. Cambridge Univ. Press, Cambridge, p. 127
Robin A. C., Reylé C., Derrière S., Picaud S., 2004, A&A, 416, 157
Skrutskie M. F. et al., 2006, AJ, 131, 1163
Smith J. A., Allam S. S., Tucker D. L., Stute J. L., Rodgers C. T., Stoughton C., 2007, AJ, submitted
Stappers B. W., van Kerkwijk M. H., Bell J. F., Kulkarni S. R., 2001, ApJ, 548, L183
Stetson P. B., 1987, PASP, 99, 191

Stetson P. B., 1994, PASP, 106, 250
Tauris T. M., 2011, in Schmidtobreick L., Schreiber M. R., Tappert C., eds, ASP Conf. Ser. Vol. 447, Evolution of Compact Binaries. Astron. Soc. Pac., San Francisco, p. 285
Tauris T. M., 2012, Science, 335, 561
Tauris T. M., 2015, Habilitation thesis, Univ. Bonn
Tauris T. M., Savonije G. J., 1999, A&A, 350, 928
Tauris T. M., Langer N., Kramer M., 2012, MNRAS, 425, 1601
van Kerkwijk M. H., Bassa C. G., Jacoby B. A., Jonker P. G., 2005, in Rasio F. A., Stairs I. H., eds, ASP Conf. Ser. Vol. 328, Binary Radio Pulsars. Astron. Soc. Pac., San Francisco, p. 357
Verbiest J. P. W. et al., 2009, MNRAS, 400, 951
Zacharias N., Finch C. T., Girard T. M., Henden A., Bartlett J. L., Monet D. G., Zacharias M. I., 2013, AJ, 145, 44

This paper has been typeset from a TEX/LATEX file prepared by the author.